Precision Measurement of the Ratio $\mathcal{B}(\Upsilon(3S) \to \tau^+\tau^-)/\mathcal{B}(\Upsilon(3S) \to \mu^+\mu^-)$

J. P. Lees,[1] V. Poireau,[1] V. Tisserand,[1] E. Grauges,[2] A. Palano,[3] G. Eigen,[4] D. N. Brown,[5] Yu. G. Kolomensky,[5] M. Fritsch,[6] H. Koch,[6] T. Schroeder,[6] R. Cheaib,[7b] C. Hearty,[7a,7b] T. S. Mattison,[7b] J. A. McKenna,[7b] R. Y. So,[7b] V. E. Blinov,[8a,8b,8c] A. R. Buzykaev,[8a] V. P. Druzhinin,[8a,8b] V. B. Golubev,[8a,8b] E. A. Kozyrev,[8a,8b] E. A. Kravchenko,[8a,8b] A. P. Onuchin,[8a,8b,8c] S. I. Serednyakov,[8a,8b] Yu. I. Skovpen,[8a,8b] E. P. Solodov,[8a,8b] K. Yu. Todyshev,[8a,8b] A. J. Lankford,[9] B. Dey,[10] J. W. Gary,[10] O. Long,[10] A. M. Eisner,[11] W. S. Lockman,[11] W. Panduro Vazquez,[11] D. S. Chao,[12] C. H. Cheng,[12] B. Echenard,[12] K. T. Flood,[12] D. G. Hitlin,[12] J. Kim,[12] Y. Li,[12] D. X. Lin,[12] T. S. Miyashita,[12] P. Ongmongkolkul,[12] J. Oyang,[12] F. C. Porter,[12] M. Röhrken,[12] Z. Huard,[13] B. T. Meadows,[13] B. G. Pushpawela,[13] M. D. Sokoloff,[13] L. Sun,[13,‡] J. G. Smith,[14] S. R. Wagner,[14] D. Bernard,[15] M. Verderi,[15] D. Bettoni,[16a] C. Bozzi,[16a] R. Calabrese,[16a,16b] G. Cibinetto,[16a,16b] E. Fioravanti,[16a,16b] I. Garzia,[16a,16b] E. Luppi,[16a,16b] V. Santoro,[16a] A. Calcaterra,[17] R. de Sangro,[17] G. Finocchiaro,[17] S. Martellotti,[17] P. Patteri,[17] I. M. Peruzzi,[17] M. Piccolo,[17] M. Rotondo,[17] A. Zallo,[17] S. Passaggio,[18] C. Patrignani,[18,§] B. J. Shuve,[19] H. M. Lacker,[20] B. Bhuyan,[21] U. Mallik,[22] C. Chen,[23] J. Cochran,[23] S. Prell,[23] A. V. Gritsan,[24] N. Arnaud,[25] M. Davier,[25] F. Le Diberder,[25] A. M. Lutz,[25] G. Wormser,[25] D. J. Lange,[26] D. M. Wright,[26] J. P. Coleman,[27] E. Gabathuler,[27,*] D. E. Hutchcroft,[27] D. J. Payne,[27] C. Touramanis,[27] A. J. Bevan,[28] F. Di Lodovico,[28,‖] R. Sacco,[28] G. Cowan,[29] Sw. Banerjee,[30] D. N. Brown,[30] C. L. Davis,[30] A. G. Denig,[31] W. Gradl,[31] K. Griessinger,[31] A. Hafner,[31] K. R. Schubert,[31] R. J. Barlow,[32,¶] G. D. Lafferty,[32] R. Cenci,[33] A. Jawahery,[33] D. A. Roberts,[33] R. Cowan,[34] S. H. Robertson,[35a,35b] R. M. Seddon,[35b] N. Neri,[36a] F. Palombo,[36a,36b] L. Cremaldi,[37] R. Godang,[37,**] D. J. Summers,[37] P. Taras,[38] G. De Nardo,[39] C. Sciacca,[39] G. Raven,[40] C. P. Jessop,[41] J. M. LoSecco,[41] K. Honscheid,[42] R. Kass,[42] A. Gaz,[43a] M. Margoni,[43a,43b] M. Posocco,[43a] G. Simi,[43a,43b] F. Simonetto,[43a,43b] R. Stroili,[43a,43b] S. Akar,[44] E. Ben-Haim,[44] M. Bomben,[44] G. R. Bonneaud,[44] G. Calderini,[44] J. Chauveau,[44] G. Marchiori,[44] J. Ocariz,[44] M. Biasini,[45a,45b] E. Manoni,[45a] A. Rossi,[45a] G. Batignani,[46a,46b] S. Bettarini,[46a,46b] M. Carpinelli,[46a,46b,††] G. Casarosa,[46a,46b] M. Chrzaszcz,[46a] F. Forti,[46a,46b] M. A. Giorgi,[46a,46b] A. Lusiani,[46a,46c] B. Oberhof,[46a,46b] E. Paoloni,[46a,46b] M. Rama,[46a] G. Rizzo,[46a,46b] J. J. Walsh,[46a] L. Zani,[46a,46b] A. J. S. Smith,[47] F. Anulli,[48a] R. Faccini,[48a,48b] F. Ferrarotto,[48a] F. Ferroni,[48a,‡‡] A. Pilloni,[48a,48b] G. Piredda,[48a,*] C. Bünger,[49] S. Dittrich,[49] O. Grünberg,[49] M. Heß,[49] T. Leddig,[49] C. Voß,[49] R. Waldi,[49] T. Adye,[50] F. F. Wilson,[50] S. Emery,[51] G. Vasseur,[51] D. Aston,[52] C. Cartaro,[52] M. R. Convery,[52] J. Dorfan,[52] W. Dunwoodie,[52] M. Ebert,[52] R. C. Field,[52] B. G. Fulsom,[52] M. T. Graham,[52] C. Hast,[52] W. R. Innes,[52,*] P. Kim,[52] D. W. G. S. Leith,[52,*] S. Luitz,[52] D. B. MacFarlane,[52] D. R. Muller,[52] H. Neal,[52] B. N. Ratcliff,[52] A. Roodman,[52] M. K. Sullivan,[52] J. Va'vra,[52] W. J. Wisniewski,[52] M. V. Purohit,[53] J. R. Wilson,[53] A. Randle-Conde,[54] S. J. Sekula,[54] H. Ahmed,[55] M. Bellis,[56] P. R. Burchat,[56] E. M. T. Puccio,[56] M. S. Alam,[57] J. A. Ernst,[57] R. Gorodeisky,[58] N. Guttman,[58] D. R. Peimer,[58] A. Soffer,[58] S. M. Spanier,[59] J. L. Ritchie,[60] R. F. Schwitters,[60] J. M. Izen,[61] X. C. Lou,[61] F. Bianchi,[62a,62b] F. De Mori,[62a,62b] A. Filippi,[62a] D. Gamba,[62a,62b] L. Lanceri,[63] L. Vitale,[63] F. Martinez-Vidal,[64] A. Oyanguren,[64] J. Albert,[65b] A. Beaulieu,[65b] F. U. Bernlochner,[65b] G. J. King,[65b] R. Kowalewski,[65b] T. Lueck,[65b] I. M. Nugent,[65b] J. M. Roney,[65b] A. Sibidanov,[65b,†] R. J. Sobie,[65a,65b] N. Tasneem,[65b] T. J. Gershon,[66] P. F. Harrison,[66] T. E. Latham,[66] R. Prepost,[67] and S. L. Wu[67]

(*BABAR* Collaboration)

[1]*Laboratoire d'Annecy-le-Vieux de Physique des Particules (LAPP), Université de Savoie, CNRS/IN2P3, F-74941 Annecy-Le-Vieux, France*
[2]*Universitat de Barcelona, Facultat de Fisica, Departament ECM, E-08028 Barcelona, Spain*
[3]*INFN Sezione di Bari and Dipartimento di Fisica, Università di Bari, I-70126 Bari, Italy*
[4]*University of Bergen, Institute of Physics, N-5007 Bergen, Norway*
[5]*Lawrence Berkeley National Laboratory and University of California, Berkeley, California 94720, USA*
[6]*Ruhr Universität Bochum, Institut für Experimentalphysik 1, D-44780 Bochum, Germany*
[7a]*Institute of Particle Physics, Vancouver, British Columbia, Canada V6T 1Z1*
[7b]*University of British Columbia, Vancouver, British Columbia, Canada V6T 1Z1*
[8a]*Budker Institute of Nuclear Physics SB RAS, Novosibirsk 630090, Russia*
[8b]*Novosibirsk State University, Novosibirsk 630090, Russia*
[8c]*Novosibirsk State Technical University, Novosibirsk 630092, Russia*
[9]*University of California at Irvine, Irvine, California 92697, USA*
[10]*University of California at Riverside, Riverside, California 92521, USA*
[11]*University of California at Santa Cruz, Institute for Particle Physics, Santa Cruz, California 95064, USA*

[12]California Institute of Technology, Pasadena, California 91125, USA
[13]University of Cincinnati, Cincinnati, Ohio 45221, USA
[14]University of Colorado, Boulder, Colorado 80309, USA
[15]Laboratoire Leprince-Ringuet, Ecole Polytechnique, CNRS/IN2P3, F-91128 Palaiseau, France
[16a]INFN Sezione di Ferrara, I-44122 Ferrara, Italy
[16b]Dipartimento di Fisica e Scienze della Terra, Università di Ferrara, I-44122 Ferrara, Italy
[17]INFN Laboratori Nazionali di Frascati, I-00044 Frascati, Italy
[18]INFN Sezione di Genova, I-16146 Genova, Italy
[19]Harvey Mudd College, Claremont, California 91711, USA
[20]Humboldt-Universität zu Berlin, Institut für Physik, D-12489 Berlin, Germany
[21]Indian Institute of Technology Guwahati, Guwahati, Assam 781 039, India
[22]University of Iowa, Iowa City, Iowa 52242, USA
[23]Iowa State University, Ames, Iowa 50011, USA
[24]Johns Hopkins University, Baltimore, Maryland 21218, USA
[25]Université Paris-Saclay, CNRS/IN2P3, IJCLab, F-91405 Orsay, France
[26]Lawrence Livermore National Laboratory, Livermore, California 94550, USA
[27]University of Liverpool, Liverpool L69 7ZE, United Kingdom
[28]Queen Mary, University of London, London E1 4NS, United Kingdom
[29]University of London, Royal Holloway and Bedford New College, Egham, Surrey TW20 0EX, United Kingdom
[30]University of Louisville, Louisville, Kentucky 40292, USA
[31]Johannes Gutenberg-Universität Mainz, Institut für Kernphysik, D-55099 Mainz, Germany
[32]University of Manchester, Manchester M13 9PL, United Kingdom
[33]University of Maryland, College Park, Maryland 20742, USA
[34]Massachusetts Institute of Technology, Laboratory for Nuclear Science, Cambridge, Massachusetts 02139, USA
[35a]Institute of Particle Physics, Montréal, Québec, Canada H3A 2T8
[35b]McGill University, Montréal, Québec, Canada H3A 2T8
[36a]INFN Sezione di Milano, I-20133 Milano, Italy
[36b]Dipartimento di Fisica, Università di Milano, I-20133 Milano, Italy
[37]University of Mississippi, University, Mississippi 38677, USA
[38]Université de Montréal, Physique des Particules, Montréal, Québec, Canada H3C 3J7
[39]INFN Sezione di Napoli and Dipartimento di Scienze Fisiche, Università di Napoli Federico II, I-80126 Napoli, Italy
[40]NIKHEF, National Institute for Nuclear Physics and High Energy Physics, NL-1009 DB Amsterdam, Netherlands
[41]University of Notre Dame, Notre Dame, Indiana 46556, USA
[42]Ohio State University, Columbus, Ohio 43210, USA
[43a]INFN Sezione di Padova, I-35131 Padova, Italy
[43b]Dipartimento di Fisica, Università di Padova, I-35131 Padova, Italy
[44]Laboratoire de Physique Nucléaire et de Hautes Energies, Sorbonne Université, Paris Diderot Sorbonne Paris Cité, CNRS/IN2P3, F-75252 Paris, France
[45a]INFN Sezione di Perugia, I-06123 Perugia, Italy
[45b]Dipartimento di Fisica, Università di Perugia, I-06123 Perugia, Italy
[46a]INFN Sezione di Pisa, I-56127 Pisa, Italy
[46b]Dipartimento di Fisica, Università di Pisa, I-56127 Pisa, Italy
[46c]Scuola Normale Superiore di Pisa, I-56127 Pisa, Italy
[47]Princeton University, Princeton, New Jersey 08544, USA
[48a]INFN Sezione di Roma, I-00185 Roma, Italy
[48b]Dipartimento di Fisica, Università di Roma La Sapienza, I-00185 Roma, Italy
[49]Universität Rostock, D-18051 Rostock, Germany
[50]Rutherford Appleton Laboratory, Chilton, Didcot, Oxon OX11 0QX, United Kingdom
[51]IRFU, CEA, Université Paris-Saclay, F-91191 Gif-sur-Yvette, France
[52]SLAC National Accelerator Laboratory, Stanford, California 94309, USA
[53]University of South Carolina, Columbia, South Carolina 29208, USA
[54]Southern Methodist University, Dallas, Texas 75275, USA
[55]St. Francis Xavier University, Antigonish, Nova Scotia, Canada B2G 2W5
[56]Stanford University, Stanford, California 94305, USA
[57]State University of New York, Albany, New York 12222, USA
[58]Tel Aviv University, School of Physics and Astronomy, Tel Aviv 69978, Israel
[59]University of Tennessee, Knoxville, Tennessee 37996, USA
[60]University of Texas at Austin, Austin, Texas 78712, USA
[61]University of Texas at Dallas, Richardson, Texas 75083, USA
[62a]INFN Sezione di Torino, I-10125 Torino, Italy

[62b]Dipartimento di Fisica, Università di Torino, I-10125 Torino, Italy
[63]INFN Sezione di Trieste and Dipartimento di Fisica, Università di Trieste, I-34127 Trieste, Italy
[64]IFIC, Universitat de Valencia-CSIC, E-46071 Valencia, Spain
[65a]Institute of Particle Physics, Victoria, British Columbia, Canada V8W 3P6
[65b]University of Victoria, Victoria, British Columbia, Canada V8W 3P6
[66]Department of Physics, University of Warwick, Coventry CV4 7AL, United Kingdom
[67]University of Wisconsin, Madison, Wisconsin 53706, USA

(Received 13 May 2020; accepted 20 October 2020; published 8 December 2020)

We report on a precision measurement of the ratio $\mathcal{R}_{\tau\mu}^{\Upsilon(3S)} = \mathcal{B}(\Upsilon(3S) \to \tau^+\tau^-)/\mathcal{B}(\Upsilon(3S) \to \mu^+\mu^-)$ using data collected with the *BABAR* detector at the SLAC PEP-II e^+e^- collider. The measurement is based on a 28 fb^{-1} data sample collected at a center-of-mass energy of 10.355 GeV corresponding to a sample of 122 million $\Upsilon(3S)$ mesons. The ratio is measured to be $\mathcal{R}_{\tau\mu}^{\Upsilon(3S)} = 0.966 \pm 0.008_{\text{stat}} \pm 0.014_{\text{syst}}$ and is in agreement with the standard model prediction of 0.9948 within 2 standard deviations. The uncertainty in $\mathcal{R}_{\tau\mu}^{\Upsilon(3S)}$ is almost an order of magnitude smaller than the only previous measurement.

DOI: 10.1103/PhysRevLett.125.241801

In the standard model (SM) the width of a spin-1 quark-antiquark bound state decaying into a charged lepton-antilepton pair is well known [1]. The ratio of widths to final-state leptons with different flavors is free of hadronic uncertainties, and for heavy spin-1 resonances, such as the family of the $b\bar{b}$ bound-state $\Upsilon(nS)$ mesons, differs from unity only by a small mass correction. Consequently, leptonic decays of the $\Upsilon(nS)$ mesons are excellent candidates to test SM predictions and search for phenomena beyond the SM. For example, the Non-SM Higgs boson A^0 proposed in Ref. [2] couples more strongly to heavier fermions and thus a larger value of the ratio $\mathcal{R}_{\tau\mu}^{\Upsilon(3S)} = \mathcal{B}(\Upsilon(3S) \to \tau^+\tau^-)/\mathcal{B}(\Upsilon(3S) \to \mu^+\mu^-)$ than that predicted by lepton-flavor universality in the SM might be observed. Recent measurements of $\mathcal{B}(B \to D^{(*)}\tau\nu)/\mathcal{B}(B \to D^{(*)}(e/\mu)\nu)$ [3] suggest a tension with the SM associated with lepton-flavor universality involving the τ lepton. It has been remarked [4] that new physics models providing an explanation for that tension also unavoidably affect the $\mathcal{R}_{\tau\mu}^{\Upsilon(3S)}$ ratio. The only measurement to date of that ratio was made by the CLEO Collaboration, $\mathcal{R}_{\tau\mu}^{\Upsilon(3S)} = 1.05 \pm 0.08 \pm 0.05$ [5]. A new precise measurement will further constrain new physics models.

We present a precision measurement of the ratio $\mathcal{R}_{\tau\mu}^{\Upsilon(3S)}$ using a novel technique to discriminate between resonant and nonresonant (i.e., continuum) dimuon production based on differences in the dimuon mass distributions associated with initial-state radiation (ISR). In the resonant process, $e^+e^- \to \Upsilon(3S) \to \mu^+\mu^-$, ISR is heavily suppressed compared to the nonresonant, $e^+e^- \to \mu^+\mu^-$, process. How we estimate the non-$\Upsilon(3S)$ contribution to the dimuon sample using this technique is detailed below. This method ensures that the measured ratio is fully inclusive of radiation effects and does not require a precise luminosity determination.

We use data collected with the *BABAR* detector at the PEP-II asymmetric-energy e^+e^- collider at the SLAC National Accelerator Laboratory. The *BABAR* experiment collected data at center-of-mass energies of the $\Upsilon(4S)$, $\Upsilon(3S)$, and $\Upsilon(2S)$ resonances, as well as at nonresonant energies. The PEP-II positron beam energy was 3.1 GeV, while the electron beam energy was 8.6 GeV at the $\Upsilon(3S)$ and 9.0 GeV at the $\Upsilon(4S)$, resulting in different boosts of the final-state system and different detector acceptances in the center-of-mass frame. We measure the ratio $R_{\tau\mu}^{\Upsilon(3S)}$ using a sample of 122 million $\Upsilon(3S)$ decays corresponding to an integrated luminosity of 27.96 fb^{-1} [6] collected at $\sqrt{s} = 10.355$ GeV during 2008 (referred to as Run-7), where $\sqrt{s}$ is the center-of-mass energy. We also employ three data control samples: data collected at the $\Upsilon(4S)$ in 2007 (referred to as Run-6) corresponding to 78.3 fb^{-1}, data taken 40 MeV below the $\Upsilon(4S)$ resonance (termed "off-resonance") corresponding to 7.75 fb^{-1}, and data taken 30 MeV below the $\Upsilon(3S)$ resonance corresponding to 2.62 fb^{-1}. All data used in this analysis were collected with the same detector configuration after the last major upgrade in 2007. These data control samples are used to evaluate properties of the background, to study systematic effects, and to calculate corrections to Monte Carlo (MC) based efficiencies. A small subset of 2.41 fb^{-1} of the total $\Upsilon(3S)$ sample is used at a pre-unblinding stage to optimize the selections.

The *BABAR* detector is described in detail elsewhere [7,8]. Charged particles are reconstructed as tracks with a 5-layer silicon vertex tracker and 40-layer drift chamber

Published by the American Physical Society under the terms of the Creative Commons Attribution 4.0 International license. Further distribution of this work must maintain attribution to the author(s) and the published article's title, journal citation, and DOI. Funded by SCOAP³.

inside a 1.5 T solenoidal magnet. An electromagnetic calorimeter (EMC) is used to identify electrons and photons. A ring-imaging Cherenkov detector is used to identify charged hadrons and provides additional electron identification information. Muons are identified by an instrumented magnetic-flux return (IFR).

The major irreducible background process is continuum dilepton production. The KKMC event generator [9] is used to simulate continuum $\mu^+\mu^-$ and $\tau^+\tau^-$ production taking into account radiative effects. For the Bhabha process the BHWIDE [10] event generator is employed. The EvtGen generator [11] is used to simulate hadronic continuum events and generic $\Upsilon(3S)$ decays, with the final-state radiation effects modeled by means of the PHOTOS package [12]. The simulated $\mu^+\mu^-$, $\tau^+\tau^-$, and generic $\Upsilon(3S)$ samples correspond to roughly twice the number of events in the $\Upsilon(3S)$ dataset, while the Bhabha sample corresponds to roughly half the number of events. In addition, the $\Upsilon(3S) \to \mu^+\mu^-$ and $\Upsilon(3S) \to \tau^+\tau^-$ signal decays are simulated using the KKMC generator with the ISR turned off. Thus the same MC generator, KKMC, is employed for both the signal and continuum, which enables a consistent evaluation of the corrections to the discrepancies between data and MC samples. This signal MC sample is about 3 times the size of the data sample. Particle interactions with the detector and its response are modeled within the GEANT4 framework [13].

Dimuon candidates have two and only two reconstructed high momentum collinear (opening angle $>160°$) charged particles in the center-of-mass frame with opposite charges and with associated EMC energy depositions consistent with the muon hypothesis. We use a polar angle acceptance in the center-of-mass frame that ensures the selection efficiency is independent of the center-of-mass energy and boost. Misidentified Bhabha events are suppressed by requiring that at least one of the muon candidates in an event has a response in the IFR. The scaled invariant mass $M_{\mu\mu}/\sqrt{s}$ of the two muons must be in the range $0.8 < M_{\mu\mu}/\sqrt{s} < 1.1$. This selection provides a dimuon sample of 18818699 events with a 99.9% purity, according to MC studies.

The $\tau^+\tau^-$ candidate selection proceeds by requiring two and only two reconstructed tracks with opposite charges in the event. One of the tracks is required to be identified as an electron based on particle identification (PID) using all detector systems, whereas the other track must fail the same electron selection requirements. Backgrounds are further suppressed by requiring the angle between the two tracks to be greater than 110° in the center-of-mass frame. The total energy registered in the EMC must be less than 70% of the initial e^+e^- energy in the laboratory frame. The acollinearity between the two tracks in the azimuthal plane must be greater than 3°. We require $|M^2_{\rm miss}/s| > 0.01$, where the missing mass, $M_{\rm miss}$, is calculated from the tracks and up to the ten most energetic EMC clusters identified as photons. The missing momentum vector must point to the sensitive part of the detector, defined as $|\cos\theta_{\rm miss}| < 0.85$ in the center-of-mass frame. To further suppress the Bhabha background, the acollinearity angle between the nonelectron track and the combination of the identified electron track and the most energetic photon must be greater than 2° in both azimuthal and polar angles in the center-of-mass frame. Two-photon backgrounds are suppressed by applying cuts that exploit correlations between the transverse momenta of the two charged particles. The selected $\tau^+\tau^-$ sample has 2173122 events with a 98.9% purity, estimated by MC studies.

The 2.62 fb^{-1} $\Upsilon(3S)$ off-resonance and 7.75 fb^{-1} $\Upsilon(4S)$ off-resonance samples are used to correct for differences between MC and data $\tau^+\tau^-/\mu^+\mu^-$ selection efficiency ratios. For the data and their corresponding MC samples, the number of dilepton candidates (MC sample scaled to the data luminosity) and corresponding efficiency corrections are shown in Table I. For the $\Upsilon(3S)$ and $\Upsilon(4S)$ off-resonance data samples, the $N_{\tau\tau}/N_{\mu\mu}$ dilepton candidate ratios are 0.11665 ± 0.00029 and 0.11647 ± 0.00017, respectively. These are in excellent agreement, demonstrating that the efficiency ratio does not depend on the center-of-mass energy or the different boosts. The corresponding MC samples show the same behavior and the average data-driven correction to the MC efficiency ratio is $C_{\rm MC} = (\varepsilon_{\tau\tau}/\varepsilon_{\mu\mu})^{\rm data}/(\varepsilon_{\tau\tau}/\varepsilon_{\mu\mu})^{\rm MC} = 1.0146 \pm 0.0016$.

The method to discriminate between $\Upsilon(3S) \to \mu^+\mu^-$ decays and the continuum production $e^+e^- \to \mu^+\mu^-$ is based on the fact that the $\Upsilon(3S)$ resonance is very narrow and thus the ISR effects are highly suppressed for the signal, but not for the continuum background. If the ISR photons have an energy greater than a few MeV (an amount associated with the spread in the PEP-II center-of-mass energy of 4 MeV coming from the spread in beam energies), then the e^+e^- interaction energy is too low to form the $b\bar{b}$ bound state. This effect results in a significant difference in the radiative tail of the $M_{\mu\mu}$ distribution for the continuum and resonance production processes for reconstructed

TABLE I. The numbers of dilepton candidates in 2.62 fb^{-1} $\Upsilon(3S)$ and 7.75 fb^{-1} $\Upsilon(4S)$ off-resonance data and MC samples and the correction for data and MC efficiency discrepancies. The numbers of MC events are scaled according to the measured luminosity.

Off-resonance sample	$N^{\rm data}_{\mu\mu}$	$N^{\rm MC}_{\mu\mu}$	$N^{\rm data}_{\tau\tau}$	$N^{\rm MC}_{\tau\tau}$	$[(N^{\rm data}_{\tau\tau}/N^{\rm data}_{\mu\mu})/(N^{\rm MC}_{\tau\tau}/N^{\rm MC}_{\mu\mu})]$
$\Upsilon(3S)$	1 538 569	1 554 208	179 466	178 569	1.015 ± 0.003
$\Upsilon(4S)$	4 422 407	4 398 983	515 067	505 133	1.014 ± 0.002

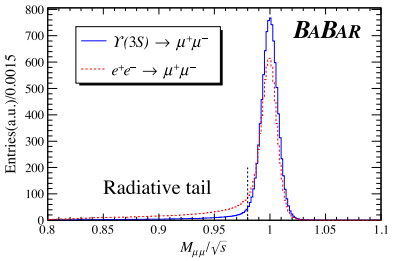

FIG. 1. Comparison of $M_{\mu\mu}/\sqrt{s}$ distributions for the continuum production $e^+e^- \to \mu^+\mu^-$ in data at the $\Upsilon(4S)$ off-resonance energy and $\Upsilon(3S) \to \mu^+\mu^-$ decays in MC simulation, where only final-state radiation is expected. The distributions are normalized to the same number of events. The vertical dashed line shows the border $M_{\mu\mu}/\sqrt{s} = 0.98$.

dimuon candidates, as shown in Fig. 1. About 23% of the continuum candidates are in the low-mass radiative tail region ($M_{\mu\mu}/\sqrt{s} < 0.98$), whereas for the resonance decays this number is 7%, and is associated with final-state radiation.

In Fig. 2 the selected events are shown for simulated $\Upsilon(3S)$ decays. For the dimuon events, the $M_{\mu\mu}/\sqrt{s}$ variable is plotted whereas for the $\tau^+\tau^-$ events the total reconstructed event energy scaled to the center-of-mass energy, $E_{\tau\tau}/\sqrt{s}$, is plotted. The total energy is evaluated using the measured momenta of the charged particles and up to the ten most energetic photons not associated with them. In the dimuon events, decays of the $\Upsilon(3S)$ to lower mass $\Upsilon(1S)$ or $\Upsilon(2S)$ resonances via radiative and hadronic transitions, where the $\Upsilon(1S)$ or $\Upsilon(2S)$ then decay into a dimuon pair, are clearly seen and separated. We refer to such processes, including analogous $\tau^+\tau^-$ final-state processes, as "cascade decays." The $M_{\mu\mu}/\sqrt{s}$ distribution provides not only an estimate of the number of $\Upsilon(3S) \to \mu^+\mu^-$ events but also a direct evaluation of the contributions from the cascade decays. In the $\tau^+\tau^-$ channel, however, these cascade decay channels are nearly indistinguishable.

In order to extract the ratio $\mathcal{R}_{\tau\mu}^{\Upsilon(3S)}$ a binned maximum-likelihood fit procedure based on the $M_{\mu\mu}/\sqrt{s}$ and $E_{\tau\tau}/\sqrt{s}$ distributions is employed using the method of Ref. [14]. The $\Upsilon(3S) \to \mu^+\mu^-$ and $\Upsilon(3S) \to \tau^+\tau^-$ templates are taken from the KKMC-based MC simulation without ISR. The templates for $\Upsilon(2S) \to \ell^+\ell^-$ and $\Upsilon(1S) \to \ell^+\ell^-$ via cascade decays, as well as the remaining small contributions from $\Upsilon(nS)$ hadronic decays, are taken from the EvtGen-based MC simulation. The continuum templates use data control samples, as described in the following paragraph.

The amount of *BABAR* data collected on-resonance is about 10 times larger than off-resonance. Consequently, when the continuum template is based only on the off-resonance data, the small size of that sample dominates the statistical uncertainty of the ratio. To overcome this limitation, $\Upsilon(4S)$ on-resonance Run-6 data, with an integrated luminosity of 78.3 fb^{-1} and the same detector configuration as Run-7, is used for the continuum template in the fit. The leptonic width of the $\Upsilon(4S)$ is 1.57×10^{-5} of its total width, which results in a negligible number of resonance-produced dilepton events being present in the sample compared to the number of continuum events. However, other $\Upsilon(nS) \to \ell^+\ell^-$ decays appear in the data continuum template via ISR. The radiative return processes have been extensively studied by *BABAR* (see, e.g., Ref. [15]) and based on this approach, the amount of ISR-produced $\Upsilon(nS)$ mesons is estimated and subtracted from the continuum template.

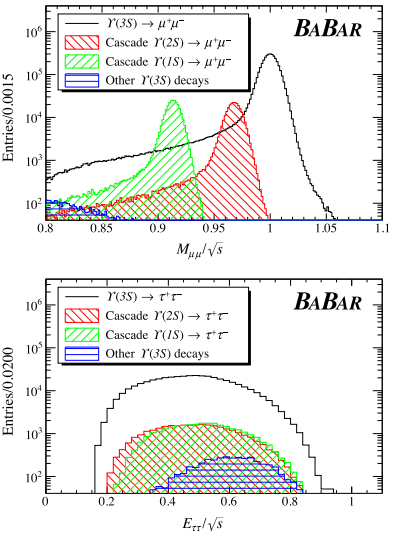

FIG. 2. Distributions of $M_{\mu\mu}/\sqrt{s}$ (top plot) and $E_{\tau\tau}/\sqrt{s}$ (bottom plot) variables in MC simulation. Cascade decays are clearly separated in dimuon events and nearly indistinguishable in $\tau^+\tau^-$ events.

The number of $\Upsilon(3S) \to \mu^+\mu^-$ events $N_{\mu\mu}$ and the raw ratio $\bar{R}_{\tau\mu} = N_{\tau\tau}/N_{\mu\mu}$ are free parameters of the fit. In the nonsignal templates, this ratio is fixed either as in data for the continuum background or to the simulation prediction for the other templates.

A graphical representation of the fit result is shown in Figs. 3 and 4. The fit yields a raw ratio of $\bar{R}_{\tau\mu} = N_{\tau\tau}/N_{\mu\mu} = 0.10778 \pm 0.00091$ and $N_{\mu\mu} = (2.014 \pm 0.015) \times 10^6$

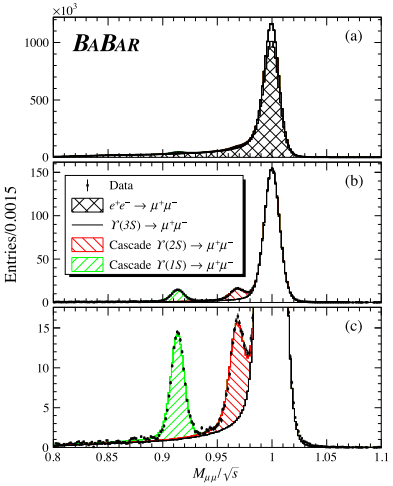

FIG. 3. The result of the template fit to the $\Upsilon(3S)$ data in the $M_{\mu\mu}/\sqrt{s}$ variable. In (a) all events are shown, in (b) and (c) the dominant continuum $e^+e^- \to \mu^+\mu^-$ background is subtracted, and (c) is a magnified view of (b) to better show cascade decays and the radiative-tail region.

events. The MC-based selection efficiencies and their ratio, required to obtain the ratio $R_{\tau\mu}$, are shown in Table II.

Low multiplicity $\Upsilon(4S) \to B\bar{B}$ decays can mimic τ-pair events and pass the selection criteria. According to MC

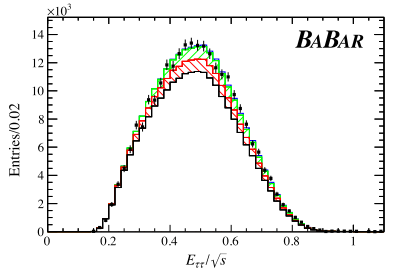

FIG. 4. The result of the template fit to the $\Upsilon(3S)$ data in the $E_{\tau\tau}/\sqrt{s}$ variable after the continuum background is subtracted. Data are depicted as points with error bars. The legend is the same as in the corresponding plot in Fig. 2.

TABLE II. MC selection efficiencies in percent for $\Upsilon(3S) \to \ell^+\ell^-$. The quoted uncertainties reflect MC statistics.

$\varepsilon_{\mu\mu}$ (%)	$\varepsilon_{\tau\tau}$ (%)	$\varepsilon_{\tau\tau}/\varepsilon_{\mu\mu}$
69.951 ± 0.018	7.723 ± 0.010	0.11041 ± 0.00015

studies, the $B\bar{B}$ contribution to the muon template is negligible whereas the $B\bar{B}$ background in the $\tau^+\tau^-$ template translates into a correction of $\delta_{B\bar{B}} = 0.42\%$ to the expected number of $\Upsilon(3S) \to \tau^+\tau^-$ candidates and is applied to the ratio $R_{\tau\mu}$.

Combining the fit result $\tilde{R}_{\tau\mu}$, the ratio of MC efficiencies $\varepsilon_{\mu\mu}/\varepsilon_{\tau\tau}$, the data/MC correction $C_{\rm MC}$, and the correction from $B\bar{B}$ events $\delta_{B\bar{B}}$, the ratio is

$$\mathcal{R}_{\tau\mu}^{\Upsilon(3S)} = \tilde{R}_{\tau\mu}\frac{1}{C_{\rm MC}}\frac{\varepsilon_{\mu\mu}}{\varepsilon_{\tau\tau}}(1+\delta_{B\bar{B}}) = 0.9662 \pm 0.0084,$$

where uncertainties from the data/MC correction and MC efficiencies are included in the statistical uncertainty.

The sources of the systematic uncertainty in $\mathcal{R}_{\tau\mu}^{\Upsilon(3S)}$ are summarized in Table III. The PID uncertainty is assessed by studying three additional $\tau^+\tau^-$ classifiers. The first used tighter electron selectors for both the τ to electron and the τ to nonelectron selection. The second applied a tighter electron selector only for the τ to nonelectron selection. The third replaced the τ to nonelectron selection with an explicit requirement that the nonelectron particle be identified as a muon or a pion. Even though the data-driven corrections associated with each of these separate $\tau^+\tau^-$ classifiers were applied, and despite the highly correlated statistics in these samples, there remains a 0.9% difference between one of these test classifiers and the default classifier, which we assign as the PID systematic uncertainty.

The ratio of the number of dimuon and $\tau^+\tau^-$ events from the cascade decays in the MC fit templates is fixed according to lepton-flavor universality. This ratio was varied according to the current experimental uncertainties in branching fractions for $\Upsilon(1S)$ and $\Upsilon(2S)$ to dimuon and $\tau^+\tau^-$ final states, resulting in a maximum difference in $\tilde{R}_{\tau\mu}$ of 0.6%, which is taken as the systematic uncertainty.

TABLE III. The summary of systematic uncertainties.

Source	Uncertainty (%)
Particle identification	0.9
Cascade decays	0.6
Two-photon production	0.5
$\Upsilon(3S) \to$ hadrons	0.4
MC shape	0.4
$B\bar{B}$ contribution	0.2
ISR subtraction	0.2
Total	1.4

The systematic uncertainty associated with two-photon background is estimated by varying the selection on the transverse momenta to reduce the $\tau^+\tau^-$ selection efficiency to almost half its nominal value. These variations result in a maximal deviation in $\bar{R}_{\tau\mu}$ of 0.5%.

The simulation of other generic $\Upsilon(3S)$ decays shows that a small fraction of background events (about 0.1% of dimuon and 1% of $\tau^+\tau^-$ samples) still pass the selection criteria. The amount of this background is fixed to the MC prediction in the fit and a 0.4% systematic uncertainty assessed by varying these backgrounds by $\pm 50\%$.

The systematic uncertainty from the MC template shape modeling associated with the radiative and resolution effects is estimated to be 0.4% based on varying the $M_{\mu\mu}$ resolution and from changing the templates based on KKMC with those using EvtGen with PHOTOS.

A systematic uncertainty of 0.2% is associated with the $B\bar{B}$ background in the continuum template, estimated by varying the expected amount of the background by $\pm 50\%$.

The systematic uncertainty associated with $\Upsilon(nS)$ mesons produced by the radiative return process in the continuum template is estimated by accounting for experimental uncertainties of total widths and leptonic branching fractions of these mesons and by varying the overall amount of these produced mesons by 10% in order to conservatively account for radiator function uncertainties. We assign a value of 0.2% as the associated systematic uncertainty.

Systematic uncertainties described in the preceding paragraphs are combined in quadrature, giving a total systematic uncertainty of 1.4%.

In conclusion, based on the data collected by the *BABAR* detector near the $\Upsilon(3S)$ and $\Upsilon(4S)$ resonances, the ratio of the leptonic branching fractions of the $\Upsilon(3S)$ meson is measured to be

$$\mathcal{R}_{\tau\mu}^{\Upsilon(3S)} = 0.966 \pm 0.008_{\text{stat}} \pm 0.014_{\text{syst}}.$$

This is 6 times more precise than the only previous measurement [5] and is within 2 standard deviations of the SM prediction of 0.9948 [4].

We are grateful for the excellent luminosity and machine conditions provided by our PEP-II colleagues, and for the substantial dedicated effort from the computing organizations that support *BABAR*. The collaborating institutions wish to thank SLAC for its support and kind hospitality. This work is supported by DOE and NSF (USA), NSERC (Canada), CEA and CNRS-IN2P3 (France), BMBF and DFG (Germany), INFN (Italy), FOM (Netherlands), NFR (Norway), MES (Russia), MINECO (Spain), STFC (United Kingdom), BSF (USA-Israel). Individuals have received support from the Marie Curie EIF (European Union) and the A. P. Sloan Foundation (USA).

[*] Deceased.
[†] Corresponding author.
sibid@uvic.ca
[‡] Present address: Wuhan University, Wuhan 430072, China.
[§] Present address: Università di Bologna and INFN Sezione di Bologna, I-47921 Rimini, Italy.
[‖] Present address: King's College, London WC2R 2LS, United Kingdom.
[¶] Present address: University of Huddersfield, Huddersfield HD1 3DH, United Kingdom.
[**] Present address: University of South Alabama, Mobile, Alabama 36688, USA.
[††] Also at Università di Sassari, I-07100 Sassari, Italy.
[‡‡] Also at Gran Sasso Science Institute, I-67100 L'Aquila, Italy.

[1] R. Van Royen and V. F. Weisskopf, Nuovo Cimento A **50**, 617 (1967); **51**, 583(E) (1967).
[2] M. A. Sanchis-Lozano, Int. J. Mod. Phys. A **19**, 2183 (2004).
[3] Y. Amhis *et al.* (HFLAV Group), Eur. Phys. J. C **77**, 895 (2017); J. P. Lees *et al.* (*BABAR* Collaboration), Phys. Rev. D **88**, 072012 (2013); M. Huschle *et al.* (Belle Collaboration), Phys. Rev. D **92**, 072014 (2015); R. Aaij *et al.* (LHCb Collaboration), Phys. Rev. Lett. **115**, 111803 (2015); **120**, 171802 (2018); G. Caria *et al.* (Belle Collaboration), Phys. Rev. Lett. **124**, 161803 (2020).
[4] D. Aloni, A. Efrati, Y. Grossman, and Y. Nir, J. High Energy Phys. 06 (2017) 019.
[5] D. Besson *et al.* (CLEO Collaboration), Phys. Rev. Lett. **98**, 052002 (2007).
[6] J. P. Lees *et al.* (*BABAR* Collaboration), Nucl. Instrum. Methods Phys. Res., Sect. A **726**, 203 (2013).
[7] B. Aubert *et al.* (*BABAR* Collaboration), Nucl. Instrum. Methods Phys. Res., Sect. A **479**, 1 (2002).
[8] B. Aubert *et al.* (*BABAR* Collaboration), Nucl. Instrum. Methods Phys. Res., Sect. A **729**, 615 (2013).
[9] B. F. L. Ward, S. Jadach, and Z. Was, Nucl. Phys. B, Proc. Suppl. **116**, 73 (2003).
[10] S. Jadach, W. Placzek, and B. F. L. Ward, Phys. Lett. B **390**, 298 (1997).
[11] D. J. Lange, Nucl. Instrum. Methods Phys. Res., Sect. A **462**, 152 (2001).
[12] E. Barberio and Z. Was, Comput. Phys. Commun. **79**, 291 (1994).
[13] S. Agostinelli *et al.* (GEANT4 Collaboration), Nucl. Instrum. Methods Phys. Res., Sect. A **506**, 250 (2003).
[14] R. J. Barlow and C. Beeston, Comput. Phys. Commun. **77**, 219 (1993).
[15] B. Aubert *et al.* (*BABAR* Collaboration), Phys. Rev. D **69**, 011103 (2004).